Editorial Manager(tm) for Solar Physics
Manuscript Draft

Manuscript Number:

Title: Signatures of the slow solar wind streams from active regions in the inner corona

Article Type: Original Research

Keywords: "Sun: corona"; "Sun: EUV imaging"; "active regions"; "solar wind: source regions"; "Differential Emission Measure"

Corresponding Author: Vladimir Slemzin, Ph.D.

Corresponding Author's Institution: P.N. Lebedev Physical Institute of RAS

First Author: Vladimir Slemzin, Ph.D.

Order of Authors: Vladimir Slemzin, Ph.D.;Louise K. Harra, Professor;Alexander Urnov, Ph.D.;Sergey Kuzin, Ph.D.;Farid Goryaev, Ph.D.;David Berghmans, Ph.D.

Abstract: Slow solar wind measured near the Earth is produced by many spatially distributed sources on the Sun. Data from the Hinode satellite revealed quasi-stationary outflows of plasma emanating from edges of active regions (ARs) (e.g. Sakao 2007). SPIRIT observations at solar maximum and TESIS and SWAP observations at solar minimum have shown that some ARs produce divergent ray-like structures (coronal rays) seen in the corona up to heights of 2-3Rsun in 1 MK iron emission lines. On the disk such ARs have fan loops seen also in 1 MK emission lines which start from outflow regions and conjugated with coronal rays appeared at the limb during solar rotation. We suggest that fan loops and coronal rays represent the signatures of plasma streams starting as outflows on the Sun, propagating along the open magnetic field lines through the inner corona and contributing to the slow solar wind. In order to investigate the link between outflows and the solar wind we analyze an isolated AR observed by TESIS, EIS and other space instruments from the end of July to the first week of August 2009. EIS detected two regions with outflow velocities V =10-30 kms-1 located in the Western and Eastern edges of the AR above the areas of low positive and negative magnetic field. The plasma temperature determined from the EIS spectral lines by the Differential Emission Measure (DEM) method had a peak at T~1 MK in both outflow regions. The fan loops seen in the Western region during its rotation to the limb were co-aligned with open magnetic field lines given by the PFSS extrapolation. However, PFSS did not show open field lines in the Eastern region. We analyzed parameters of the solar wind measured in different time intervals by STEREO-B, ACE, Wind and STEREO-A and found that the solar wind density projected to the Carrington longitudes of the AR was well correlated with longitudinal distribution of the outflow flux density determined by EIS.

Solar Physics
DOI: 10.1007/•••••-•••-•••-••••-•

Signatures of the slow solar wind streams from active regions in the inner corona

V. Slemzin[1] · **L. Harra**[2] · **A. Urnov**[1]
S. Kuzin[1] **F. Goryaev**[1,3] **D. Berghmans**[3]

Abstract Slow solar wind measured near the Earth is produced by many spatially distributed sources on the Sun. Data from the *Hinode* satellite revealed quasi-stationary outflows of plasma emanating from edges of active regions (ARs) (e.g. Sakao *et al.*, 2007). SPIRIT observations at solar maximum and TESIS and SWAP observations at solar minimum have shown that some ARs produce divergent ray-like structures (coronal rays) seen in the corona up to heights of 2–3$R_{\rm sun}$ in 1 MK iron emission lines. On the disk such ARs have fan loops seen also in 1 MK emission lines which start from outflow regions and conjugated with coronal rays appeared at the limb during solar rotation. We suggest that fan loops and coronal rays represent the signatures of plasma streams starting as outflows on the Sun, propagating along the open magnetic field lines through the inner corona and contributing to the slow solar wind. In order to investigate the link between outflows and the solar wind we analyze an isolated AR observed by TESIS, EIS and other space instruments from the end of July to the first week of August 2009. EIS detected two regions with outflow velocities V = 10–30 km s^{-1} located in the Western and Eastern edges of the AR above the areas of low positive and negative magnetic field. The plasma temperature determined from the EIS spectral lines by the Differential Emission Measure (DEM) method had a peak at $T \sim 1$ MK in both outflow regions. The fan loops seen in the Western region during its rotation to the limb were co-aligned with open magnetic field lines given by the PFSS extrapolation. However, PFSS did not show open field lines in the Eastern region. We analyzed parameters of the solar wind measured in different time intervals by *STEREO-B*, *ACE*, *Wind* and *STEREO-A* and found that the solar wind density projected to the Carrington longitudes of the AR was well correlated with longitudinal distribution of the outflow flux density determined by EIS.

[1] P.N. Lebedev Physical Institute, Leninsky Pr., 53, Moscow, 119991, Russia. email: slem@sci.lebedev.ru
[2] UCL-Mullard Space Science Laboratory, Holmbury St Mary, Dorking, Surrey, RH5 6NT, UK. email: lkh@mssl.ucl.ac.uk
[3] Royal Observatory of Belgium, Ringlaan 3, 1180 Brussels, Belgium. email: david.berghmans@oma.be

1. Introduction

Since the discovery of the solar wind detection of its sources became one of the main fundamental problems of solar physics. It is believed that the quasi-stationary solar wind has two main components – the fast solar wind dominating at solar minimum, and the slow solar wind dominating at solar maximum. Early studies of the X-ray solar images on *Skylab* (Levine *et al.*, 1977) and later measurements of the solar wind with *ULYSSES* and *ACE* (Gosling *et al.*, 1995; McComas *et al.*, 2001) have shown that the fast solar wind at the solar maximum originates from polar coronal holes (PCH). The fast speed wind remains steady, whereas the slow wind is intermittent. Although it is ordinarily believed that the main causes of the wind intermittency are plasma turbulence and interaction of high and slow speed wind, there are suggestions that fluctuations of the quasi-stationary slow wind may be generated in lower corona or be a result of movement of its sources during solar rotation. Analysis of *ULYSSES* and *ACE* data have shown that in different phases of the solar cycle the slow wind emanates from various local source regions, such as boundaries of PCH and equatorial coronal holes (ECH) (Neugebauer *et al.*, 1998; Neugebauer *et al.*, 2002; Liewer, Neugebauer, and Zurbuchen, 2003; Liewer, Neugebauer, and Zurbuchen, 2004; Wang, Ko, and Grappin, 2009), helmet streamers (Sheeley *et al.*, 1997) and active regions (ARs) (Hefti *et al.*, 2000; Liewer *et al.*, 2001). In general, sources of the slow solar wind are not as well understood as coronal holes and hence theoretical modeling of the slow solar wind is not as developed.

The source regions of the quasi-stationary solar wind are identified by using measurements of the solar wind near the Earth and applying two different methods. The first is the ballistic back-tracking method described firstly by Nolte and Roelof (1973) and developed further in the more sophisticated Wang-Sheeley-Arge (WSA) model (Wang and Sheeley, 1990). The back-tracking method is based on two main assumptions: (1) the solar wind moves between the solar surface and so-called "source surface" (SS) at $R = 2.5R_{\rm sun}$ along divergent commonly non-radial open magnetic field lines; (2) between the SS and the Earth it propagates along radial open magnetic field lines with constant speed equal to its value measured near the Earth. The magnetic field in the inner corona is usually extrapolated on the basis of synoptic maps of the photospheric magnetic field using the Potential Field Source Surface model (PFSS model – Schatten, Wilcox, and Ness, 1969; Wang and Sheeley, 1992; Schrijver and De Rosa, 2003). The back-tracking method typically provides the longitudinal accuracy $\sim 10^0$ at the source surface, 3–5^0 at the Sun. The latitudinal correspondence is within $\pm 10^0$. The main uncertainty originates from inaccuracy of the computed structure of the coronal magnetic field because PFSS is based on synoptic maps of the photospheric magnetic field rarely updated only at the visible side of the Sun whereas many large loops end on the invisible back side (Nitta and De Rosa, 2008).

The second method frequently applied to identify the type of the solar wind source regions is by analyzing specific solar wind parameters measured in situ near the Earth such as the solar wind velocity, ionic composition and temperature. It is now well established (see, e.g., Raymond *et al.*, 1997; von Steiger *et*

al., 2000; Neugebauer *et al.*, 2002; Strachan *et al.*, 2002; Bemporad *et al.*, 2003; Liewer, Neugebauer, and Zurbuchen, 2004; Ko *et al.*, 2006; Wang, Ko, and Grappin, 2009) that such parameters as "frozen-in temperature" (or corresponding O^{7+}/O^{6+} ratio) and the FIP (first ionization potential) bias determined as a proxy by the Fe/O ratio, sufficiently differ for two types of magnetic configurations inherent to the specific solar wind sources: open field structure of coronal holes (CH) or closed field structure of active regions (AR). In some intermediate cases these parameters indicate that the source is located in the interface region between AR and adjacent CH or the resulting solar wind flux is a mixture of flows from ARs and CHs located at different latitudes but at near the same longitude.

Localization of the slow solar wind sources may be achieved by high resolution mapping of outflow fluxes at the solar disk with the use of the Doppler spectroscopy. Outflows from the Sun are often detected in different solar structures by the Doppler shifts of spectral lines. Uchida *et al.* (1992) reported the detection of outflows from active regions observed in X-rays as continual expansion of the loops. Švestka *et al.* (1998) observed fans of transient coronal rays above ARs after flares and suggested that they may contribute to the solar wind. In both cases outflows lasted for periods from several hours to several days. Winebarger, DeLuca, and Golub (2001) observed long lasting outflows in the TRACE 171 Å images with velocities between 5 and 20 km s^{-1}. Data from the XRT telescope aboard *Hinode* (Golub *et al.*, 2007) showed a continuous outflow of plasma along open magnetic field lines emanating from the edge of an AR located adjacent to a coronal hole (Sakao *et al.*, 2007). Brightness variations along a fan-like structure showed velocities of 100–170 km s^{-1} with a temperature of 1.1 MK. The mass loss rate from this AR was estimated to be about $\sim 1/4$ of the total mass loss rate of the solar wind. The same event was analyzed spectroscopically by the *Hinode*/EIS instrument (Culhane *et al.*, 2007). Harra *et al.* (2008) found coronal outflow with the projected velocity $V \sim 50$ km s^{-1} originated from the same place where fan rays were observed with the XRT telescope.

Not all outflows detected spectroscopically leave the Sun as some of them may be just a part of common "coronal circulation" of the solar plasma (Marsch *et al.*, 2008). A study of structure of the inner solar corona in the range $R = 1 - 2R_{\rm sun}$ can help us to determine coronal signatures of open magnetic configurations which potentially may be tracers of the slow solar wind. This range of the inner corona plays an important role as the intermediate region where magnetic field is restructuring from closed to open configurations but it is not studied in detail so far. Coronagraphs on spacecraft systematically obtain moderate quality images of the corona in white light (WL) at the distances above $2R_{\rm sun}$. The ground-based instruments can produce high quality images of the corona from the limb to $R = 6-10R_{\rm sun}$ only during very short eclipse observations. Depending on solar activity, the WL corona contains two or more low contrast streamers summarized from many weak features along the line of sight irrespective of their temperature. Methods of gradient filtering reveal the fine structure of streamers which correspond to a gradient of integrated brightness of the K-corona rather than to localized magnetic structures. In contrast, the EUV corona is observed in the ionic spectral lines excited in a limited temperature range evidently related with

specific local magnetic structures. Independently on the prevailing mechanism of excitation for a given spectral line - collisional or resonant scattering (which is debated now) - the EUV corona is better fits for localization of the solar wind sources.

The first EUV observations of the inner corona in the 175 Å band containing Fe IX – Fe XI lines up to the radial distances $R = 2-3R_{\rm sun}$ were carried out with the SPIRIT telescope aboard the *CORONAS-F* satellite (Slemzin *et al.*, 2008) at solar maximum. These observations revealed extended ray-like structures appeared above some active regions when they rotated to the limb. At solar minimum coronal rays were observed in 2009 with the TESIS telescope in 171 Å band (Kuzin *et al.*, 2009). Currently coronal rays are observed with the SWAP telescope (Berghmans *et al.*, 2006) onboard the *PROBA2* satellite in the 174 Å band. These observations have shown that coronal rays often appear at the limb above active regions which contain fan loops when seen at the disk in the 1 MK coronal lines. Hence, it is reasonable to hypothesize that coronal rays and fan loops may be the signatures of outflows in the inner corona.

The aim of this work is to investigate possible relationship between outflows from active regions and coronal structures - fan loops and coronal rays, as probable signatures of coronal streams which may contribute to the quasi-stationary solar wind observed near the Earth. We describe existing data on properties of coronal rays at solar maximum and at low solar activity. We summarize the main properties of outflows from active regions based on the data of previous studies and examine the relationship between outflows, coronal structures and the slow solar wind for an active region observed in July–August 2009 with various space solar instruments. For this case we analyze the EIS intensity and velocity maps, study the temperature structure of the emitting plasma in the outflow regions using the Differential Emission Measure (DEM) method, and compare coronal signatures of outflows with computed magnetic field configurations. Finally, we consider the solar wind data measured by *STEREO-B*, *ACE*, *Wind* and *STEREO-A* for the case under study and analyze their possible correlation with the EIS data on outflows. Discussion and conclusion sections will summarize the results.

2. Coronal rays in the inner corona at solar maximum and minimum

Ordinary EUV telescopes can observe the solar corona only to the distances $R < 1.3 - 1.5R_{\rm sun}$ due to the limited field of view and insufficient sensitivity to exponentially decaying coronal brightness. On the other hand, most of WL coronagraphs cannot see the corona below $2R_{\rm sun}$ (e.g. LASCO C2 and C3 coronagraphs – Brueckner *et al.*, 1995) or have too low spatial resolution to resolve its fine structure (Mauna Loa MK4 – Burkepile, Darnell, and Tomczyk, 2005). SPIRIT was the first EUV telescope to have a special coronagraphic mode, in which the direct disk radiation was suppressed by using an external occulter which allowed to study a large part of the inner corona from the solar surface to the radial distance of $2.5–3R_{\rm sun}$ (Slemzin *et al.*, 2008). The successor of SPIRIT, the TESIS EUV telescope (Kuzin *et al.*, 2009), operated in February–November 2009, also was able to see the inner corona using a tiltable mirror

and wide range of exposure times from tens of second to 600 s. Both SPIRIT and TESIS had very low straylight due to their one-mirror Herschel optical design. The SWAP EUV telescope, which observes the corona since 2010, has a design of one-quarter of the EIT telescope with one spectral channel 174 Å (Defise *et al.*, 2007). The telescope is able to observe the whole inner corona in a special "paving" multiple exposures mode, when the satellite tilts the main axis on ~ 10 arcmin sequentially in 4 positions (North-East, South-East, North-West and South-West). In each position the telescope takes 80–90 images with a cadence of 30 s. The images in each paving position are summed and then combined together to obtain a whole image of the inner corona. The SWAP off-pointing is limited to 3^0. Typically we see the signal up to 2 $R_{\rm sun}$ from the disc center. The main limitations are straylight and dark current noise.The straylight was extrapolated from radial brightness distribution in periphery regions of the image above $R > 2R_{\rm sun}$ and subtracted.

Figure 1 shows images of the inner corona in the Fe IX – Fe XI band taken by SPIRIT (175 Å Fe IX – Fe XI lines) at solar maximum (December 5, 2002) and by SWAP (174 Å Fe IX – Fe X lines) at low solar activity (July 8, 2009). At solar maximum coronal rays are seen as bright structures originating from some active regions and super-radially extending to distances more than $2R_{\rm sun}$. Most of the rays have an angular spread of several degrees, in some cases their angular width was as much as 30^0. The mid-latitude rays are declined poleward. At the distances $R > 1.5R_{\rm sun}$ above the closed loops coronal rays had high brightness (up to 2–4 times) with respect to the surrounding diffuse (non-resolved) corona.

At solar minimum coronal rays are seen as a bundle of thin threads diverging super-radially from active regions and declining on angles up to $\sim 60^0$ and more. In Figure 2 there is a SWAP composite image taken on 11 July 2010, at 02:57:29 - 06:11:59 UT in comparison with the WL image taken with on-ground telescope during the eclipse of July 11, 2010 at 18:42 UT (courtesy of Serge Koutchmy and Jean Mouette, Institut d'Astrophysique de Paris, CNRS and UPMC, France). Most of coronal rays seen in EUV are bounded with active regions and rotated with them whereas the extended streamers seen in WL are not definitely associated with any specific structures at the Sun.

Often, if not always, the appearance of coronal rays at the limb is preceded by existence of specific fan-like structures which are seen at the disk at periphery of the same active regions and are conjugated with coronal rays in the course of the solar rotation. From analysis of the *TRACE* (Schrijver *et al.*, 1999) and EIT (Berghmans *et al.*, 1999) images it was proposed that these structures are cool loops with temperatures $T \sim 1$ MK or below. Based on the *TRACE* and *HINODE*/XRT and EIS data Ugarte-Urra, Warren, and Brooks (2009) described peripheral extended loop-like structures with temperatures $T \sim 0.9$–1.3 MK showing brightness variations interpreted as downflows with velocities $V \sim 39$–105 km/s. Recently Warren *et al.* (2011) reported that outflows determined from the EIS spectroscopic data are observed primarily in the emission lines from Fe XI – Fe XV. It was suggested that outflows lie on open magnetic field lines that connect to the heliosphere. In contrast, bright fan-like structures seen in colder transition region lines are dominated by downflows. Ugarte-Urra and Warren (2011) found that the Fe XII 195.119 Å blueshifted spectral profiles

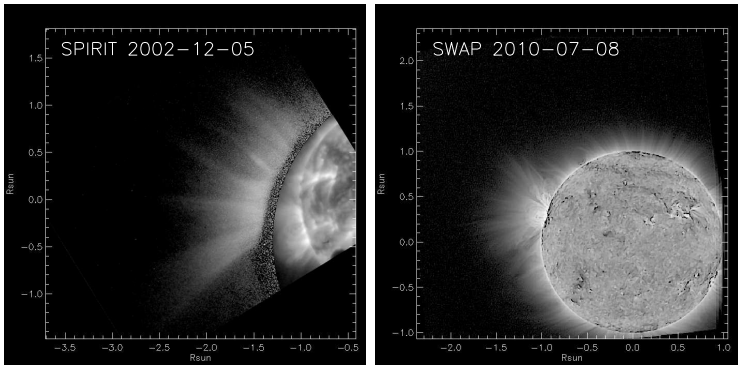

Figure 1. Images of the inner corona in the Fe IX – Fe XI lines taken by SPIRIT at solar maximum (December 5, 2002) and by SWAP at solar minimum (July 8, 2010).

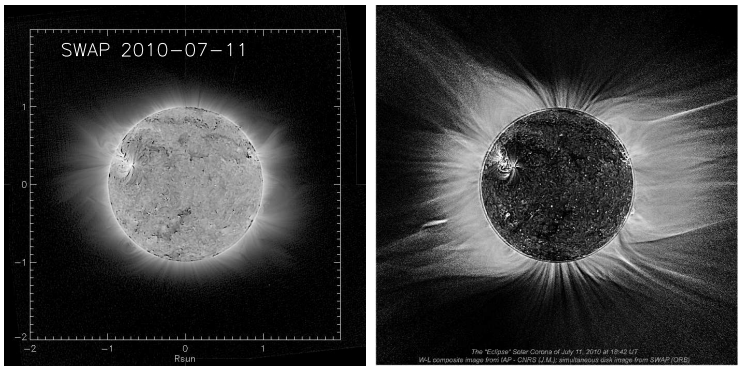

Figure 2. Images of the Sun taken in the eclipse July 11, 2010. Left panel: the SWAP image registered on 02:57:29–06:11:59 UT. Right panel: the WL image registered during the main phase of the total eclipse of July 11, 2010 at 18:42 UT, combined with the SWAP image taken at the same time (courtesy of Serge Koutchmy and Jean Mouette, Institut d'Astrophysique de Paris, CNRS and UPMC, France).

at their footpoints exhibit transient blue wing enhancements corresponding to outflows on timescales of 5 min cadence with velocities of 40–130 km/s. Brooks, Warren, and Young (2011) analyzed together the data of EIS and *SDO*/AIA (Golub, 2006) by means of the DEM method and confirmed that a number of fan loops have peak temperatures of 0.8–1.2 MK.

Results of these studies pointed out that at least two classes of fan structures exist in active regions: colder structures with temperatures $T \sim 0.6$–0.8 MK dominated by downflows and hotter structures with $T \sim 0.8$–1.2 MK showing in some cases downflows in other - outflows. The outflowing structures are more natural to be named as "fan rays" but here we will name it here traditionally as "fan loops". However, observations in most cases show only lower parts of these structures, and their identification as "closed" or "open" is based on their curvature or co-alignment with extrapolated magnetic field lines given by the PFSS method which is known to be not correct in showing open field lines within active regions (Nitta and De Rosa, 2008). There are some open questions

concerning interpretation of fan loops or rays. It is difficult to explain some of their features found by Schrijver *et al.* (1999) and Winebarger, DeLuca, and Golub (2001) : why they are not seen in the middle part of the AR and what is the origin of plasma moving outward along them.

Summarizing the main properties of the coronal rays from observations at solar maximum and minimum we can conclude that:

- some active regions have bright coronal rays seen in the EUV range at the limb up to $R = 2 - 3R_{\rm sun}$;
- at distances $R > 1.5R_{\rm sun}$ coronal rays are seen with the highest contrast in the Fe IX – Fe XI lines excited at the temperature $T \sim 1$ MK whereas structures in hotter lines (e.g. in the *SOHO*/EIT images in the 195 Å and 284 Å bands), mostly closed loops, are seen at lower heights;
- coronal rays are typically originated in the boundaries of active regions, in particular, in the regions adjacent to coronal holes;
- coronal rays appear at the limb in the course of the solar rotation being conjugated with fan loops seen at the disk in 1 MK spectral lines;
- some of the coronal rays had counterparts in the LASCO C2 WL images as isolated rays or elements of the helmet streamer. Typically, there is no full correspondence between the brightness of the rays and brightness of the WL streamer.

3. Outflows measured by the Doppler shifts of the coronal spectral lines

Since *Hinode* was launched, there has been increasing interest in understanding the strong outflow regions at the edges of active regions. Sakao *et al.* (2007) observed the outflow to be in steady streams of plasma that reach speeds of 100 km s^{-1}. Harra *et al.* (2008) analyzed the main line Doppler shifted profiles and found speeds of around 50 km s^{-1}, which when corrected for the magnetic field orientation, reached speeds similar to those seen in the imaging data. This confirms that the fan structures seen at the edges of active regions may be associated with upflowing plasma. The creation and maintenance of the outflowing plasma is not clearly understood yet. The main issue is whether the upflowing plasma measured by EIS, does actually leave the Sun and form part of the slow solar wind. There have been various suggestions as to what could create this upflowing plasma. This includes reconnection over large spatial scales, which is consistent with the low curvature of the fan structure. Harra *et al.* (2008) showed through magnetic field extrapolation, how the edges of the active regions can reconnect with bipoles lying further away from the active region. Baker *et al.* (2009) suggested that the outflowing material lies predominantly at regions where there is a strong change in the orientation of the magnetic field (e.g. between an open and closed magnetic field line). They found that the strongest upflows were co-located with quasi-separatrix layers. Another option to explain the outflows was put forward by Murray *et al.* (2010) who studied the special case of an active region inside a coronal hole. In this case they found through simulations that

the outflow could be replicated through the process of compression. The outflows measured from the coronal spectral lines could indicate probable source regions of the slow solar wind. Not all outflowing plasma leaves the Sun, some of them may indicate siphon plasma flows or flows along large loops. To understand whether the observed outflow contributes to the solar wind or not, one needs to investigate its properties and presence of other signatures indicating its propagation to the larger distances like coronal rays.

4. Case study of the active region in July-August 2009

We investigate the relationship between outflows at the Sun and their coronal signatures by studying an isolated active region observed at the solar disk from July 25 to August 8, 2009. The active region, not numbered by NOAA (hereafter we will name it 'AR'), was observed on July 28 by the *STEREO-B* EUVI telescope (Howard *et al.*, 2008) at the center of the disk (Figure 3). The structure of the AR consisted of a system of loops extended in the South-East to North-West direction. Fan loops marked by the arrows in Figure 3 were seen in the Western and Eastern edges of this structure being the brightest in the 171 Å line.

During the period from July 25 to August 9 this AR was observed by the EUV instruments *SOHO*/EIT (Delaboudiniere *et al.*, 1995), *TRACE* (Handy *et al.*, 1999), *CORONAS-Photon*/TESIS (Kuzin *et al.*, 2009), *Hinode*/XRT (Golub *et al.*, 2007) and EIS (Culhane *et al.*, 2007) at close to the central meridian on August 1.

At this stage, the structure of the AR observed in the 171 Å band had not changed significantly compared with that observed by *STEREO-B* on July 28, including two fan loop bundles marked by the arrows. TESIS observed the Sun starting from August 1, 11:26:40 UT. The AR was observed from the beginning of this day until the start time of the TESIS observations by XRT, EIT and *TRACE*. EIS scanned the AR, in a range of emission lines, from 01:22:14 to 02:57:14 UT. Figure 4 shows *Hinode*/XRT full disk image taken on August 1, 2009 at 06:21:03 UT with the outlined region of interest (ROI) (a), the zoomed ROI taken from the XRT image at 01:23:44UT (b) and the *TRACE* image in 195 Å taken at 01:23:19 UT at the beginning of the EIS scan (c).

A sequence of images taken by the *Hinode*/XRT telescope between 00:00 and 08:00 show a flare peaking at 03:02 UT accompanied with a loop expansion. The light curve of the XRT total intensity in the ROI from 00:00 to 08:00UT is shown in Figure 4 (d). Figure 5 shows a series of EIT images in 195 Å taken at the beginning of the EIS scan (01:23:17 UT, (a)), after maximum of the flare (03:11:34 UT (b)) and near the beginning of the TESIS observations (11:47:17 UT, (c)). The panel (d) shows the difference image at 04:35:17 UT – 01:23:17 UT with the dimming appeared after the flare below region 2. It seems, that the flare did not affected the fan loops at the edges of the AR.

4.1. EIS observations

We analyzed the AR on August 1, 2009 with data from the EUV Imaging Spectrometer (EIS, Culhane *et al.*, 2007) on the *Hinode* spacecraft (Kosugi *et al.*,

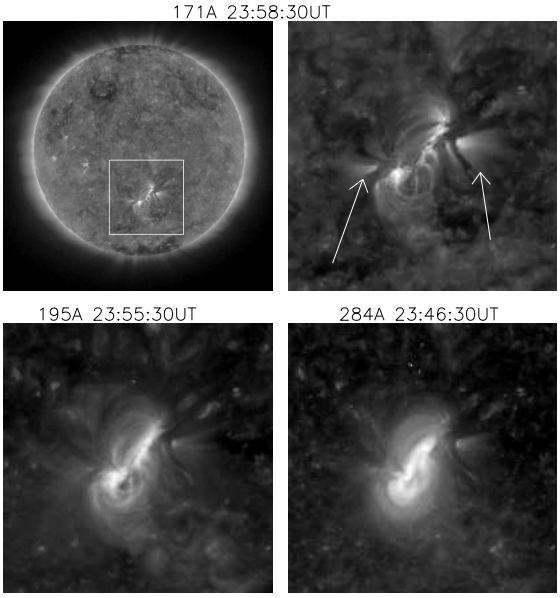

Figure 3. Images of the AR taken by *STEREO-B* EUVI on July 28, 2009. Arrows indicate fan loops.

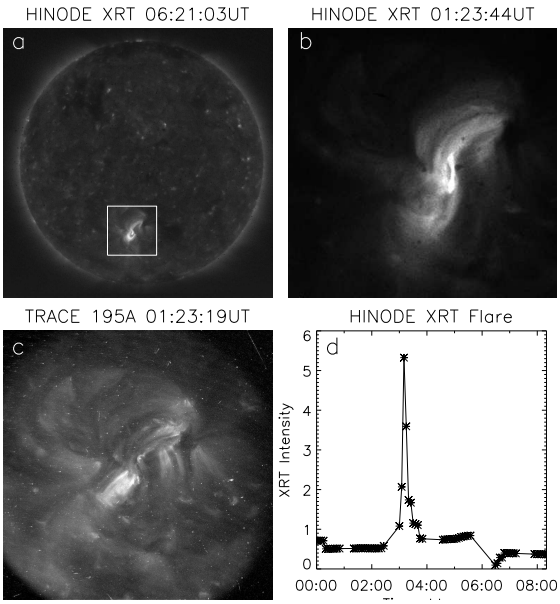

Figure 4. *HINODE*/XRT full disk image with Al/Ti-filters taken on August 1, 2009 at 06:21:03 UT (a). The zoomed AR area taken from the XRT image at 01:23:44UT (b). The *TRACE* image in 195 Å taken at 01:23:19 at the beginning of the EIS scan (c). The X-ray light curve measured by XRT in the ROI from 00:00 to 08:00UT including the flare peaked at 03:02UT (d).

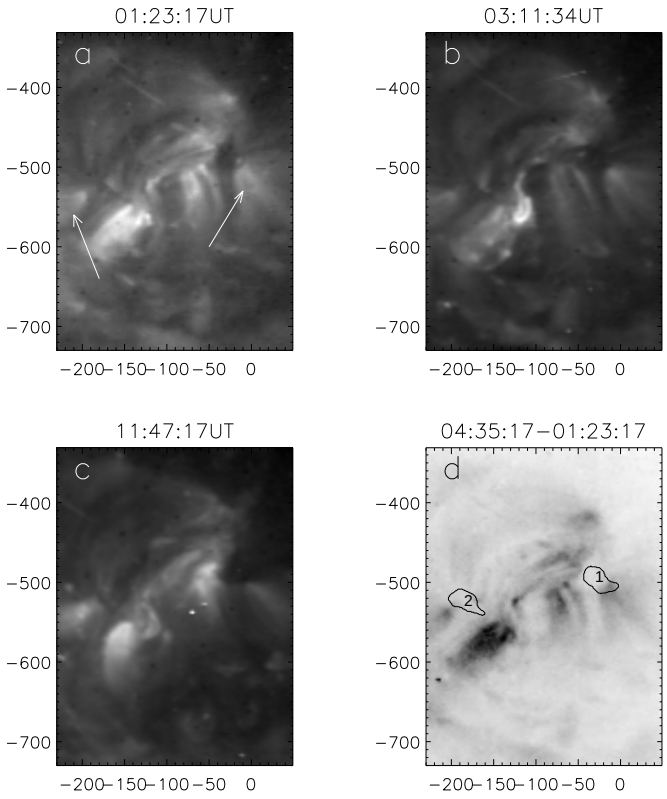

Figure 5. EIT images in 195 Å taken on August 1, 2009 at the beginning of the EIS scan (01:23:17 UT)(a), after maximum of the flare (03:11:34 UT) (b) and near the beginning of the TESIS observations (11:47:17 UT) (c). EIT difference image showing a dimming after the flare at 04:35:17 UT (d). The contours outline regions 1 and 2 determined by EIS (see section 4.1). Arrows indicate fan loops.

2007). The EIS instrument observes in two wavebands: 170–210 Å and 270–290 Å. It has four slit/slot positions: 1″, 2″, 40″, and 266″. In this paper we will analyze data taken with the 2″ slit and using the fine mirror movement to 'raster' and build up an image. The standard calibration was used and the emission lines were fitted with a Gaussian profile in order to measure the intensities and Doppler shifts.

Figure 6 shows an intensity image derived from the EIS Fe XII emission line. The time axis is also shown to illustrate how the EIS image is built up with time, so we can understand when the flare occurred during the raster. The flare started when the raster was towards the left side of the frame and hence the AR structure observed during the EIS scan was undisturbed.

The outflows in active regions have been found to be higher for higher temperature lines as described by Del Zanna (2008) . In order to investigate this dependence in our case we selected the regions in the Fe XII velocity map where the outflow velocities exceed 10 km s^{-1}. The intensity and Doppler velocity

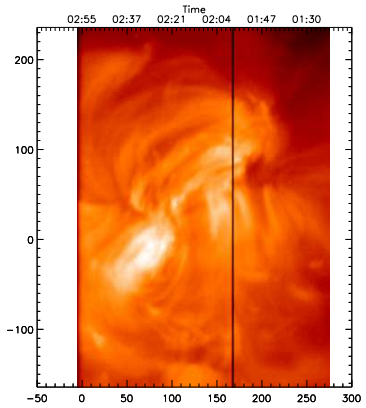

Figure 6. The EIS intensity image derived by fitting the Fe XII emission line. The x and y axis show the spatial scale in arcsecs. Since the image is derived by "rastering" from right to left, the time axis is shown on top.

maps are shown in Figure 7 for the Fe X, Fe XII, Fe XIII, Fe XIV and Fe XV lines. The areas of two biggest regions in the Fe XII line are contoured and marked by numbers '1' and '2'. The velocity histograms for all ions are shown in the two right columns. The emission becomes weaker as the temperature of the plasma increases, but the Doppler velocity increases from Fe X to Fe XIII and then decreases for Fe XIV and Fe XV. The size of the areas where outflow exceed 10 km s^{-1} follows this dependence. It should be noted that in all cases the highest velocities are concentrated in the central parts of these areas which are spatially correlated in all lines. However the outflowing velocities are weak, not exceeding 30 km s^{-1}in projection to the line-of-sight. Although the signal statistics for the highest ions Fe XIV and Fe XV in the region 2 is lower than that in the region 1, the principal dependence of velocity on the ionization state is the same for both regions. The fan loops marked by arrows in Figures 3 and 5 are most clearly seen in the intensity of the Fe X emission line.

Analysis of the velocity maps has shown that distribution of velocities along the fans is different for the Fe X and Fe XII – Fe XV lines. In the Fe X line in both regions the fan loops start from boundaries of the outflow regions (marked from Fe XII map) with the velocities V $\sim$ (-5)$\div$(-7) km s^{-1}, then the velocities raise up to V $\sim$ 3$\div$5 km $s^{-1}$and gradually fall down to zero. The average length of the fans is 40 – 60 Mm. In the Fe XII – Fe XV lines the velocities are negative along the full length of a fan gradually decreasing from (-10)$\div$(-15) km $s^{-1}$to zero. We would remind that negative velocity corresponds to outflow, positive - to downflow.

A study of a sequence of the EIT images in 195 Å after the EIS scan (Figure 5) has shown that region 1 was not disturbed by the flare. The structure of the AR

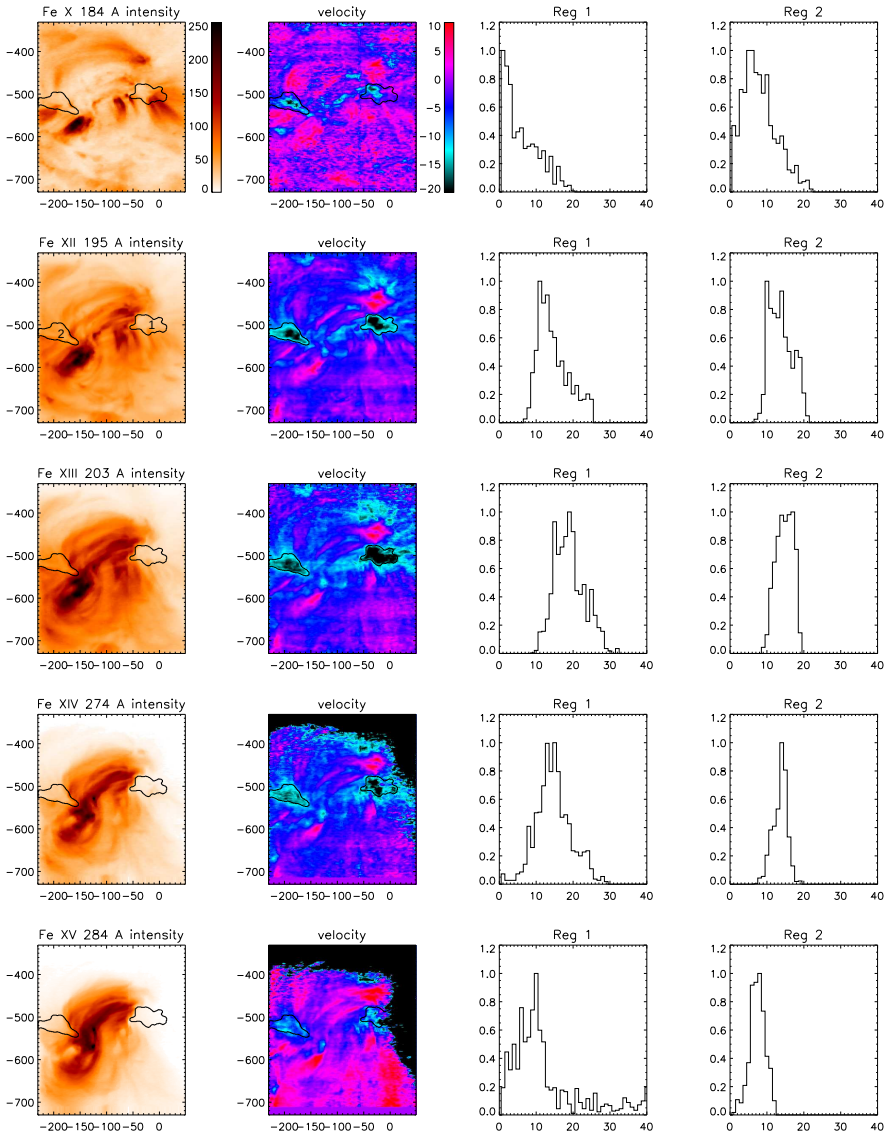

Figure 7. The Fe X, Fe XII, Fe XIII, Fe XIV and Fe XV intensity and Doppler velocity maps for the 1 August 2009 raster. The blue colour shows the upflowing plasma, and the red colour shows the downflowing plasma. The contours correspond to the largest outflow regions defined from the Fe XII velocity map by the condition $|V| > 10$ km s^{-1}.

around region 2 has changed after the flare, in particular, a dimming appeared at the same longitude southwest from region 2. We cannot verify that region 2 remained or disappeared after this evolution and only suggest that the dimming may also contribute to the total outflow at the time when this longitude crossed the central meridian.

4.2. DEM analysis of plasma temperature distributions

A comparison of plasma temperature distributions that characterize the coronal plasma structures involved in some dynamical process gives important information about their possible relationship. In particular, by using the DEM analysis one can determine whether involved coronal structures have the same temperature behavior or not. In the case under study we applied the DEM analysis to different areas in the AR to explore the properties of the outflow plasma in comparison with other coronal regions.

For the DEM analysis we used the diagnostic technique developed within the framework of the probabilistic approach to the spectral inverse problem for determining the temperature content of the emitting plasma sources (see Urnov *et al.*, 2007; Goryaev *et al.*, 2010). The probabilistic approach uses the language of the probability theory and mathematical statistics and is formulated in terms of distribution functions, hypotheses, confidence level etc. This technique called Bayesian iterative method (BIM) is an iterative procedure based on Bayes' theorem and is used to reconstruct DEM distributions. The BIM has proven to be effective in solving a series of problems such as the image restoration, the signal recovery of noisy data, the deconvolution of initial X-ray spectra recorded by Bragg spectrometers, as well as the DEM temperature analysis of both X-ray spectra from tokamak plasma and EUV solar spectra and imaging data from space experiments (Goryaev *et al.*, 2010). In particular, DEM studies of temperature profiles using the BIM showed multi-temperature character of coronal plasma structures and gave an example when the traditionally used diagnostic approach based on the filter ratio method leads to substantial errors in temperature and emission measure determination (Urnov *et al.*, 2007). Furthermore, this reconstruction method has been deduced in a regular way on the basis of Bayes' theorem, and, in contrast to the algebraic optimization techniques, does not need any regularization constraints. The BIM algorithm also provides the ultimate resolution enhancement (super-resolution) as compared with linear and other non-parametric methods (see Gelfgat, Kosarev, and Podolyak, 1993, and references therein). The latter property allows the BIM to reconstruct fine temperature structures in the DEM profiles where other DEM techniques derive smoothed and less informative solutions.

A number of recent works has used the DEM analysis to explore different regions of the Sun observed by means of the EIS instrument. The temperature structure of quiet Sun (QS) regions was analyzed in the papers by Matsuzaki *et al.* (2007) , Warren and Brooks (2009) and Brooks *et al.* (2009) . Matsuzaki *et al.* (2007) analyzed EIS observations of typical quiet regions and an active region deriving emission measure maps. They found out the high temperature components, consisting of a group of loops at temperatures of $\sim$ 1 MK and

$\sim$ 2 MK superposed in the line of sight, and the low temperature component at $\sim$ 0.4 MK. Warren and Brooks (2009) presented an analysis of temperature and density measurements above the limb in the quiet corona using the EIS data, and Brooks *et al.* (2009) carried out a DEM analysis of the quiet solar corona on the disk. For both cases the authors found the plasma temperature component peaked near 1 MK. In Landi and Young (2009) the authors reported on a cold, bright portion of an active region observed by the EIS instrument. The emitting region was characterized by a large maximum at $\log T \approx 5.6$, corresponding to transition region temperatures, and a broad tail in the DEM distribution extending to higher temperatures. Brooks and Warren (2011) have studied the outflow regions of AR 10978 for establishing a connection between active region outflows and the solar wind. They measured in particular the electron density and temperature in the outflows and obtained average values of $\log N_e = 8.6$ and $\log T = 6.2$. In a recent work by Brooks, Warren, and Young (2011) the authors investigated the temperature structure of active region fan loops using combined *Hinode*/EIS and *SDO*/AIA data. They specifically found the DEM distributions to be peaked near temperatures of 0.8–1.2 MK.

We applied our DEM diagnostics technique to a few areas in the AR which are displayed as boxes of 10×10 pixels on the Fe XII intensity map in Figure 8 (left panel). The measured intensity fluxes in EIS spectral lines were obtained using the standard EIS solarsoft. The corresponding EIS lines are listed in Table 1. In this table $T_{\max}$ is the temperature of the maximum abundance for each ion (Mazzotta *et al.*, 1998). For calculations of the contribution functions we used CHIANTI database (version 6.0.1 – Dere *et al.*, 1997; Landi *et al.*, 2006). The DEM analysis was performed adopting the ion fractional abundances of Mazzotta *et al.* (1998) and the coronal elemental abundances of Feldman *et al.* (1992) .

In order to calculate the contribution functions, we also carried out electron density measurements using line ratios. There are a number of density-sensitive line ratios in the EIS wavelength ranges (see, e.g., Young *et al.*, 2009). For the density diagnostics we used the Fe XII λ186.88/λ195.12 ratio sensitive in the range of densities $\log N_e \approx$ 8–12 cm^{-3}. The evaluated values of densities for the solar areas under study are found to be $\log N_e \approx$ 8.4–9 cm^{-3}.

Figure 8 shows results of our DEM calculations for few solar areas: outflow regions and fan loops (middle panel), loop and quiet solar region (right panel). The spectra from the quiet solar region was used to determine the reference Doppler velocity . In all cases we selected in the DEM profiles three temperature components: $\log T \sim$ 5.5–5.6, $\log T \sim$ 5.9–6.0, and $\log T \sim$ 6.1–6.2. All the recovered DEM profiles have low temperature components at temperatures of $\log T \approx$ 5.5–5.6 ($\sim$ 0.4 MK). This corresponds to the solar transition region temperatures and originates from the fact that plasmas of different temperatures are superimposed along the line of sight on the solar disk. The high temperature component in closed loops has significantly larger emission measure at $\log T \approx 6.2$ than at temperatures of $\log T \approx 6.0$. The DEM distribution for the QS region demonstrates that the high temperature component at $\log T \approx$ 6.1–6.2 exceeds the middle peak at $\log T \approx$ 5.9–6.0.

Table 1. List of the EIS lines used in the DEM analysis.

Ion	λ , Å	$\log T_{max}$	Ion	λ , Å	$\log T_{max}$
Fe X	184.54	6.0	Fe XIII	203.83	6.2
Fe XII	186.88	6.1	Fe XIII	203.80	6.2
Fe XI	188.23	6.1	Fe XII	203.72	6.1
Fe XI	188.30	6.1	Fe VIII	186.60	6.0
Fe XII	192.39	6.1	Fe X	257.26	6.0
Fe XI	192.83	6.1	Fe XIV	264.79	6.2
O V	192.90	5.4	Fe XIV	274.20	6.2
Fe XII	195.12	6.1	Si VII	275.35	5.8
Fe XII	195.18	6.1	Fe XV	284.16	6.3
Fe XIII	202.04	6.2	Fe XIV	257.39	6.3

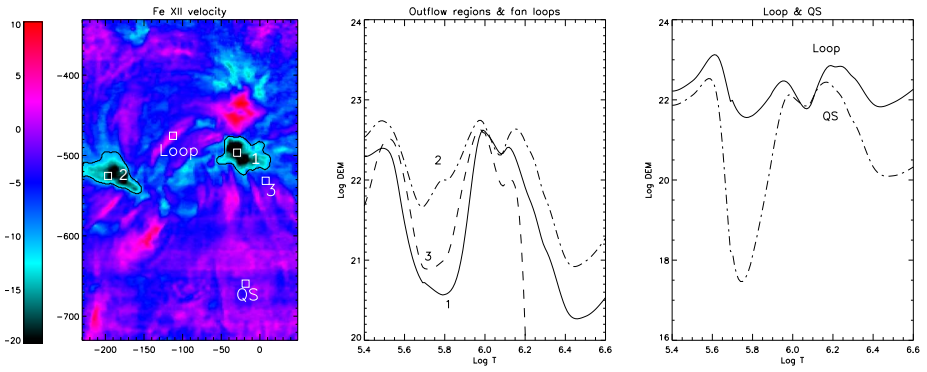

Figure 8. Different structures indicated by boxes on the Fe XII velocity map (left panel) and their DEM functions: 1 and 2 - outflow regions, 3 - fan loops, Loop - closed hot loops, QS - quiet Sun.

In both outflow regions (middle panel in Figure 8) the plasma contains all three temperature components. The medium temperature component $\log T \approx 6.0$ is the largest indicating that the plasma at temperatures of ≈ 1 MK prevails in the outflow regions. The high temperature component $\log T \approx 6.2$ (≈ 1.5 MK) is less profound than in closed hot loop structures. However, the hotter component is weaker in the fan loops than in the outflow regions.

4.3. Magnetic field in the outflow regions

The magnetic field map obtained at the ground-based Big Bear observatory on August 1, 2009 at 01:22UT is shown in Figure 9 (left panel). The photospheric magnetic field had a simple dipole configuration being negative at the Eastern end and positive at the Western end. The middle and right panels display correspondence between outflow velocities and the line-of-sight magnetic field strength in the regions 1 and 2 shown by contours. The outflow plasma from the AR near the solar surface presumably propagates along open field lines radially

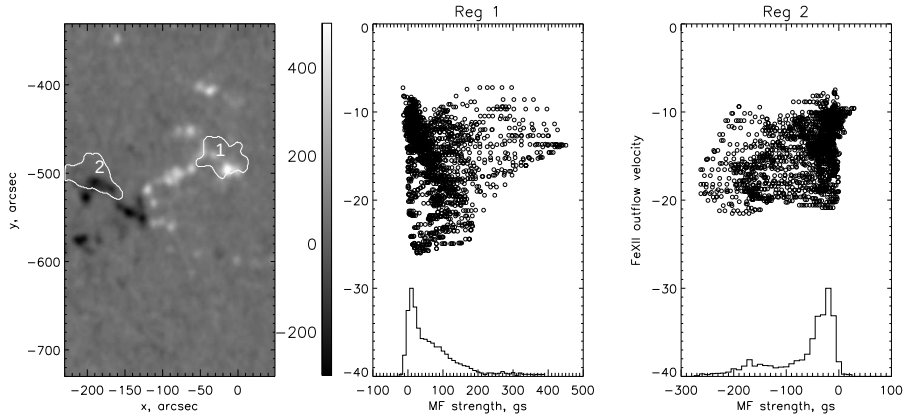

Figure 9. Photospheric magnetic field from the Big Bear observatory data (left panel), and distribution of outflow velocities in dependence on magnetic field in the regions 1 (middle) and 2 (right). The contours corresponding to the outflow velocities in the Fe XII line more than 10 km $s^{-1}$are shifted upward to compensate the projection effect. The graphs in the bottom show the normalized distributions of the total velocity flux on the magnetic field strength.

directed at the latitudinal angle -32^0. We assume that the EIS velocity map corresponds to the median height $h \approx 25$ Mm which is a half of the scale of height for $T \sim 1$ MK and compensated a displacement between the velocity and photospheric magnetic field maps by shifting the velocity map upward on 18 pixels. The velocity/magnetic field histograms in Figure 9 show that the outflow regions 1 and 2 are located in the places of relatively low ($|B| < 100$ Gs) magnetic field nearby the regions of the stronger field ($|B|_{\max} \approx 300$–400 Gs). Our result disagrees with the conclusion of Marsch, Wiegelmann, and Xia (2004) that the outward mass flows correspond to a negative polarity of the field while the inward mass flows are associated with a positive polarity of the field. In our case outflows were observed above magnetic field condensations of both signs.

The structure of the magnetic field in the AR obtained by the PFSS extrapolation is shown in Figure 10. In the western part of the AR two types of field lines are seen: open field lines with positive polarity and many very long closed loops, some of them end in the northern polar coronal hole. We suggest that open field lines may originate as a result of reconnection of some of these long loops with the interplanetary open magnetic field. In the eastern part there are no open field lines are seen amongst a bundle of very long loops. This does not contradict the presence of outflow in region 2 if we take into consideration that PFSS often do not show open field lines inside active regions and cannot take into account probable reconnection of some large loops with the interplanetary magnetic field at the back side of the Sun.

Figure 10 shows the evolution of coronal structures in the vicinity of the AR, observed by TESIS in 171 Å as the active region rotated towards the Western limb. At the beginning (August 1 12:00) fan loops originated from the outflow regions and are seen in the projection on the disk. During the period from August 1 to August 8 several small flares or brightenings occurred in the AR but the fan loops remained. On August 8–9, where the AR was at the Western limb, the

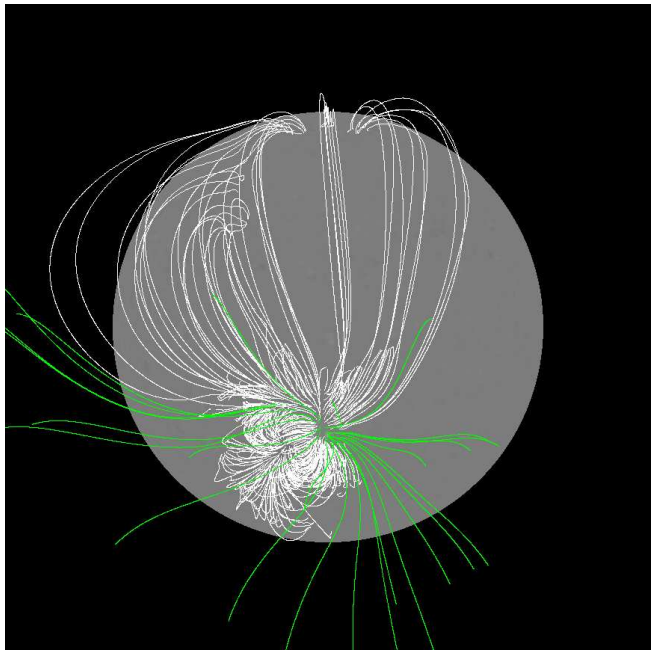

Figure 10. PFSS extrapolation of magnetic field in the AR for August 1, 2009, 00:04UT. Closed magnetic field lines are marked by white, open lines (positive) – by green color.

coronal rays appeared at the places of the former fan loops. During this period the fan loops and coronal rays were co-aligned with open field lines.

5. Analysis of solar wind data and possible imprints of outflows

To identify possible imprints of outflows from the studied AR to the solar wind we analyzed the solar wind parameters measured by instruments on several satellites: by SWEPAM, SWICS and MAG on *ACE* and SWE on *Wind* at the Lagrangian L1 point (McComas *et al.*, 1998; Gloeckler *et al.*, 1998), PLASTIC on *STEREO-B* and *STEREO-A* at their orbital positions displaced from the Sun-Earth line. In the simple ballistic model the solar wind measured by a space-based instrument may be tracked back to some source region at the SS with the time delay of $\Delta T = L_{S-E}/V_r$, where L_{S-E} is the distance between the SS and the spacecraft and V_r is the measured solar wind velocity. Then the source region at the SS is projected to the Sun using the computed configuration of the coronal magnetic field.

If we take a typical velocity of slow solar wind $V \sim 400$ km s^{-1}, the expected time delay for *ACE* will be $\Delta T \sim 4$ days. The AR crossed the Sun-Earth plane between DOY 213 and 214 of 2009, so its impact to the solar wind may be detected by *ACE* between DOY 217 and 218 (August 5-6, 2009). Figure 11 (a-d) shows the *ACE*/SWEPAM data for the solar wind density N_{H^+} and velocity V_{H^+} and SWICs data for ionic ratios O^{7+}/O^{6+} and Fe/O averaged over the

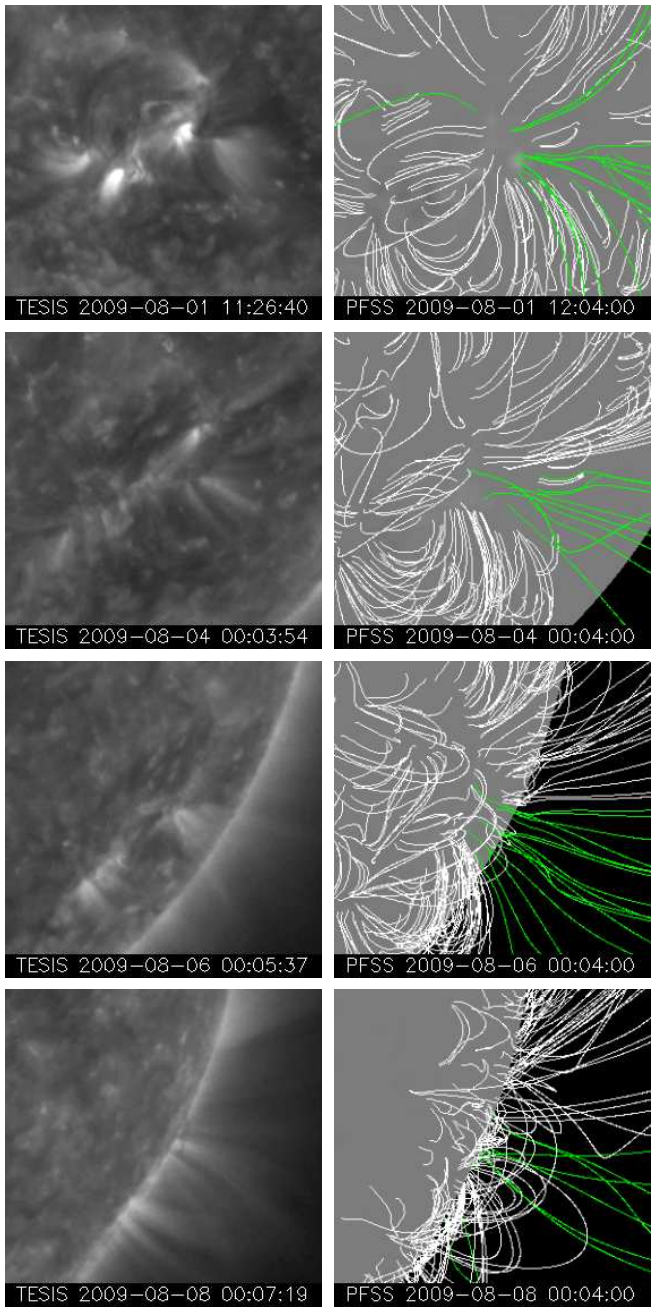

Figure 11. Evolution of the AR seen by TESIS in the 171 Å band and PFSS extrapolation for August 1 to August 8, 2009 (all times are in UT). Closed magnetic field lines are marked by white, open lines – by green color.

2h interval. The data before 217.5 and 217.4 for the latter two parameters were missing. Between DOY 217 and 218 the solar wind velocity was ≈ 380 km s^{-1}and raised up to about 500 km s^{-1}on DOY 218.2 due to arrival of high speed wind from the coronal hole northward from the AR. The solar wind density had two peaks at DOY 217.4 and 218.0. The compression peak corresponding to the interaction between slow and high speed solar wind components was not pronounced. The O^{7+}/O^{6+} ratio was 0.17–0.26 which suggests the intermediate case between active region and coronal hole sources according to Liewer, Neugebauer, and Zurbuchen (2004) . After DOY 218.2 it fell down to ≤ 0.05 which is a typical value for coronal holes. The averaged Fe/O ratio over the 217–218 day period is 0.096 which is smaller than it should be in the case of active region (> 0.25) and even less than the typical value for the streamer belt wind at solar minimum (0.09–0.13).

Variations of the GSM components of the interplanetary magnetic field measured by the *ACE*/MAG instrument (Figure 12(e)) correspond to position of the IMF sector boundary near the Sun-Earth plane during the *ACE* observations accompanied by polarity reversal of the mean solar magnetic field (see the WSO data, $http://wso.stanford.edu/meanfld/$). Nevertheless, polarity of the radial x-component remained positive during most of the time interval.

Temporal variations of the solar wind velocity and density corresponding to the Carrington longitudes of the AR were studied using the data obtained from *STEREO-B* on DOY 214-216 (August 2-4), from *ACE* and *Wind* on DOY 217-219 (August 5-7) and from *STEREO-A* on DOY 221-223 (August 9-11). Figure 13, upper panel, shows velocity of the solar wind measured by four satellites at different times, transposed to the solar surface and presented in the unified temporal scale for observer at the Earth. The *ACE* and *Wind* data fully agree between themselves as well as *STEREO-B* and *STEREO-A*. The difference between the data of two pairs of satellites may be partly explained by the difference in their latitudinal positions (Veselovsky and Shugay, 2010). Based on averaged velocities over the observational intervals, we determine the following time delays for bounding the data to the solar longitudes: for *ACE* and *Wind* - 4.2 days, for *STEREO-B* - 5.6 days, for *STEREO-A* - 5.1 days. These time delays are accurate within 0.1 day which is confirmed by a temporal coincidence of the stream interfaces in the upper panel of Figure 13. Using these time delays we transposed the measured data to the Carrington longitudes and compared the solar wind density at the same longitudes for different time intervals (Figure 13, middle panel).

The bottom panel in Figure 13 shows the latitudinal distribution of the outflow flux density obtained from the EIS Fe XII data. We determined the outflow flux density as $F_{out} = V_{out} \cdot (I_{\mathrm{FeXII}})^{1/2}$, where V_{out} is the absolute value of the outflow velocity and the square root of the Fe XII line intensity is used as a proxy for density of the outflow plasma. To obtain a longitudinal distribution we integrated the outflow flux density over latitude in the EIS field of view. For integration we selected only pixels with $V_{out} > 10$ km s^{-1} corresponding to the regions 1 and 2 in Figure 7.

We found that longitudinal distributions of the solar wind density in all time intervals contain three components peaked at the longitudes of 249, 239.6 and

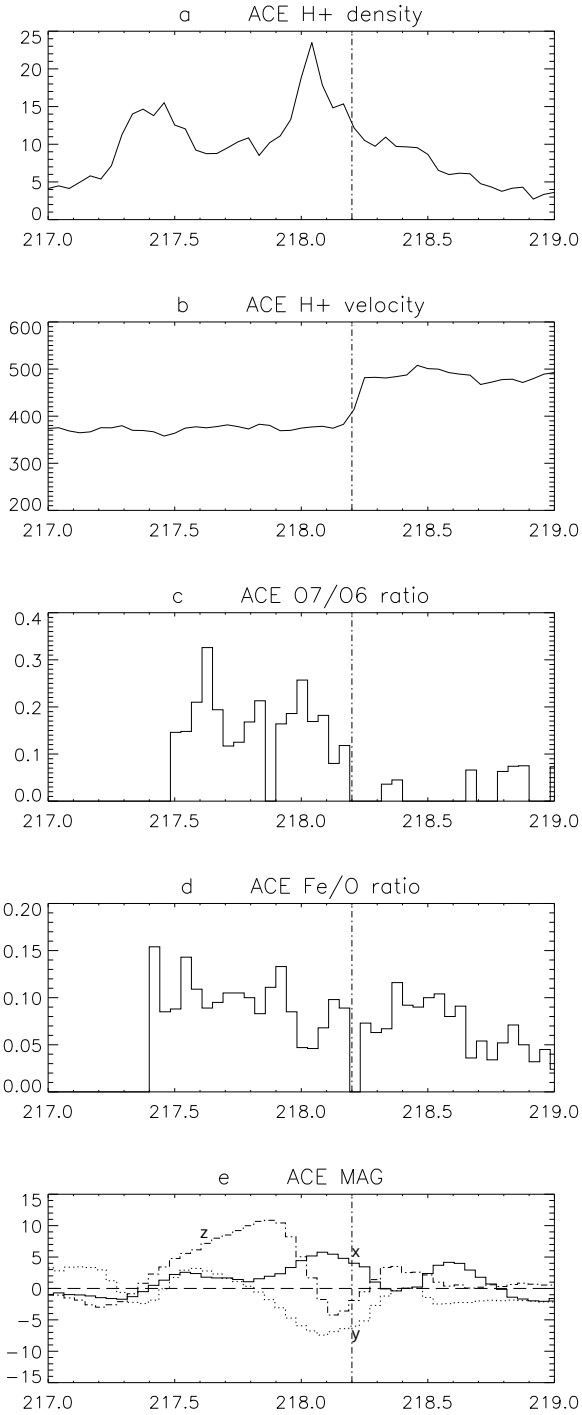

Figure 12. *ACE* solar wind data in the period between DOY 219 and 219, 2009 (August 5–7, 2009). The dashed line corresponds to the stream interface at the time of the HSS arrival.

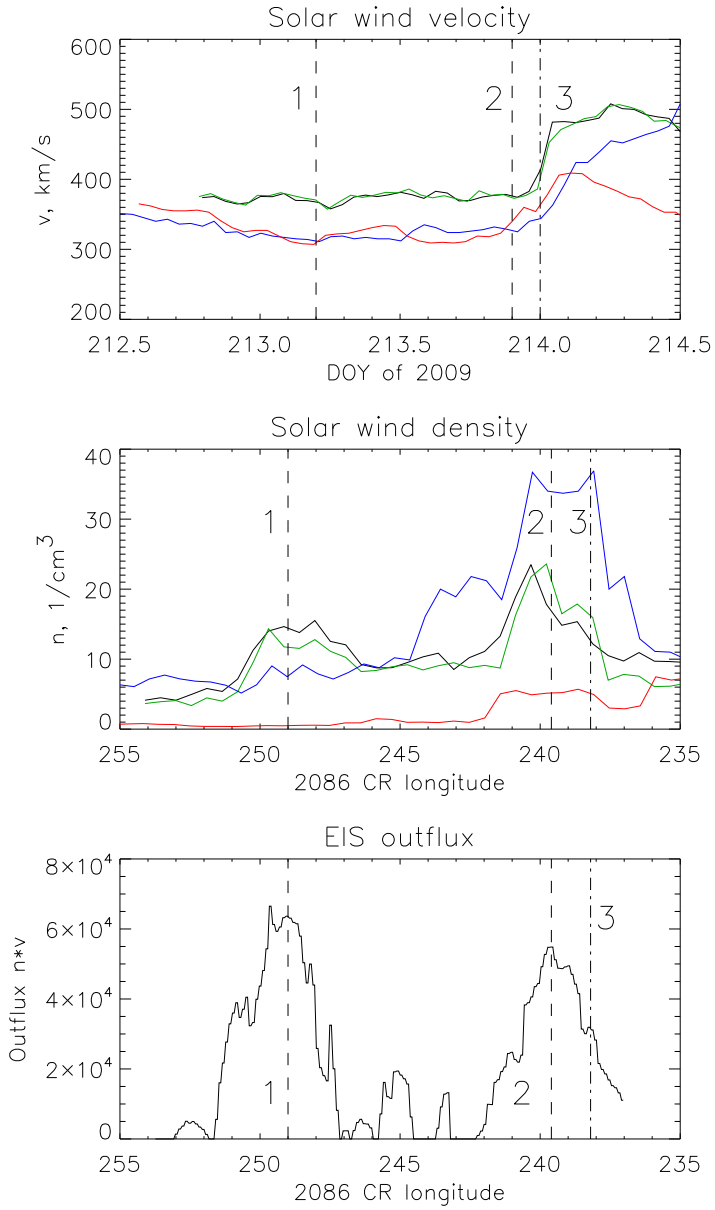

Figure 13. Top panel: solar wind velocities measured by *ACE* (black line), *Wind* (green line), *STEREO-B* (red line) and *STEREO-A* (blue line) at the moments corresponding to the same longitudes in the time scale of the Earth's observer. Middle panel: the solar wind density measured by *ACE*, *Wind*, *STEREO-B* and *STEREO-A* as the function of the Carrington longitudes. Bottom: the longitudinal dependence of the outflux density determined from the EIS Fe XII data. Numbers 1 and 2 correspond to longitudes of centers of the outflow regions 1 and 2, 3 - to boundary of the northern coronal hole.

238.2 degrees (marked in Figure 13 by numbers 1,2 and 3). The peaks 1 and 2 are well correlated in longitude with peaks of the outflow flux density. The amplitudes of these peaks are sequentially growing with time from *STEREO-B* to *ACE/ Wind* and then to *STEREO-A*. The peak 3 corresponds to the western boundary of the coronal hole and appearance of high speed wind at DOY 214 at the top panel of Figure 13.

6. Discussion

The results of this study allow us to make assumptions about 3D geometry and properties of outflows in ARs and their coronal signatures. Most assumptions about origin of outflows in ARs are based on reconnection-related mechanism: expansion of loops that lie above active region reconnecting with other loops or the interplanetary magnetic lines (Harra *et al.*, 2008), interaction between horizontally expanded active region and adjacent coronal hole (Murray *et al.*, 2010), emergence of serpentine-like magnetic flux providing reconnection with surroundings or compression (Harra *et al.*, 2010). Some other mechanisms can produce temporal or quasi-periodic flows: jet or spicule-like events (McIntosh and De Pontieu, 2009), coronal mass ejection providing outflow from dimming region (Harra *et al.*, 2011) but the latter is unlikely to produce a long-lasting slow wind. Based on analysis of the EIS velocity map and the computed magnetic field configuration in the AR and in the global scale, we assume that in the case of August 1, 2009 the outflows originated in the legs of large-scale loops and propagate along open field lines, which possibly appeared as a result of interchange reconnection between high cool loops and open heliospheric magnetic field lines (Baker *et al.*, 2009).

There are suggestions that loops consist of fine filamentary isothermal structures with different temperatures (DeForest, 2007). Such loops after reconnection may transform into a bundle of thin thread-like open funnels through which plasma is flowing out. In contrast with closed multi-temperature loops, the outflowing plasma in open funnels has a temperature within the narrow range around 1MK with a minor admixture of hotter plasma of $\sim$1.6 MK. The hotter component is responsible for radiation in the lines of Fe ions higher than Fe X. This fine structure of temperature distribution was revealed only due to high sensitivity and accuracy of our DEM probabilistic method.

We supposed that the initial coronal signatures of outflows at the disk are fan loops. Some authors (e.g. Ugarte-Urra, Warren, and Brooks, 2009, Warren *et al.*, 2011) suggest that fan structures are parts of cool loops indicating downflows. In our case we found different behavior: in the Fe X line, where the fan structures are the brightest, the fans indicate outflows in their origin, downflows in the middle and then disappear. In the lines of higher Fe-ions from Fe XII to Fe XV outflows are observed along all length of the fans with the absolute value of velocity gradually decreasing from 10 - 15 to several km s^{-1}. To explain these results, we suppose that fan structures consist of threads with different temperatures. The colder threads seen in the Fe X line are closed loops, the hotter seen in the Fe XII to Fe XV lines are open ray-like structures. Our suggestion agrees with the

conclusion of Warren *et al.*, 2011 that outfows are observed primarily in in the Fe XI to Fe XV emission lines. They also suggested that the fans, which are often associated with outfows,are not directly related to the active region outflows. In addition to this statement we suggest that fan loops observed in the Fe X line contain plasma escaping from the main outflow and falling down to the Sun and hereby represent indirect signatures of outflows. The hotter fan loops (rays) represent outflows along open field lines. This suggestion is supported by the fact that the temperature distribution of plasma in fan loops is similar to that in the outflow regions which confirms a genetic relationship between these structures.

Our analysis of the case of August 1-8, 2010 has shown that in the course of the solar rotation fan loops rooted in outflow regions of the AR conjugated with extended coronal rays at the western limb. Spectroscopic properties of coronal rays are similar to that of fan loops: both structures are better observed in the 1 MK EUV spectral lines. Del Zanna and Mason (2003) have shown that large-scale coronal structures seen in the *TRACE* 173 Å band have narrow temperature distribution around 1 MK similar to that found in fan loops by many researchers and in our case. Based on these reasons we suggest that fan loops and coronal rays represent different signatures of the same coronal structure displaying a transit of outflowing plasma in the corona through open magnetic field lines.

We believe that the observed high correlation between longitudinal distributions of the solar wind density and the outflow flux density confirms that outflows in active regions seen by Doppler shifts of the coronal lines may contribute to the slow solar wind. Temporal variations of the solar wind densities observed by instruments on different spacecrafts may be explained by variations of outflows from the solar sources as well as by latitudinal shift of the solar wind.

7. Conclusion

Based on the results of our study we determined that the main coronal signatures of outflows from active regions are fan loops at the disk and extended coronal rays at the limb seen in the 1 MK coronal spectral lines and co-aligned with open magnetic field lines. In the case of AR observed by EIS on August 1, 2010, parameters of the solar wind measured in different intervals by several spacecrafts were correlated in time with spatial distribution of outflows in the AR. In particular, the solar wind density measured by *STEREO-B*, *ACE*, *Wind* and *STEREO-A* projected to the the Carrington longitudes of the AR had peaks coincided with enhancements in outflow flux density determined by EIS.

Acknowledgements We are very grateful to Serge Koutchmy for providing the IAP eclipse picture, Nariaki Nitta, Andrey Zhukov and Igor Veselovskii for useful discussions. *Hinode* is a Japanese mission developed and launched by ISAS/JAXA, collaborating with NAOJ as a domestic partner, NASA and STFC (UK) as international partners. Scientific operation of the *Hinode* mission is conducted by the *Hinode* science team organized at ISAS/JAXA. This team mainly consists of scientists from institutes in the partner countries. Support for the post-launch operation is provided by JAXA and NAOJ (Japan), STFC (U.K.), NASA (U.S.A.), ESA, and NSC (Norway). We are grateful to NASA, ESA and the *TRACE* and

STEREO teams for their open data policy. *SOHO* is a project of international cooperation between ESA and NASA. The *CORONAS-Photon*/TESIS data were provided by the team of the Laboratory of X-ray Astronomy of the Sun of the P.N. Lebedev Physical Institute of Russian Academy of Sciences. We thank the *ACE* SWEPAM and SWICS instrument teams and the *ACE* Science Center for providing the *ACE* data. The WIND SWE experiment is a collaborative effort of Goddard Space Flight Center (GSFC), University of New Hampshire (UNH), and Massachusetts Institute of Technology (MIT). This work was supported by the FP-7 SOTERIA Project of the European Commission and the *PROBA2* Guest Investigation Grant. SWAP is a project of the Centre Spatial de Liege and the Royal Observatory of Belgium funded by the Belgian Federal Science Policy Office (BELSPO). The work was partially supported by the Grant 11-02-01079 of the Russian Foundation for Fundamental Research and the Grant OFN-15 of the Russian Academy of Sciences.

References

Baker, D., van Driel-Gesztelyi, L., Mandrini, C. H., Démoulin, P., and Murray, M. J.: 2009, *Astrophys. J.* **705**, 926.
Bemporad, et al.: 2003.
Berghmans, D., Clette, F., et al.: 1999, ESA **SP-448**, 575.
Berghmans, D., Hochedez, J.F., et al.: 2006, *Adv. Space Res.* **38**, 1807.
Brooks, D.H., et al.: 2009, *Astrophys. J.* **705**, 1522.
Brooks, D.H. and Warren, H.P.: 2011, ApJ Lett. **727**, L13.
Brooks, D.H., Warren, H.P., and Young, P.R.: 2011, *Astrophys. J.* **730:85**, 13pp.
Brueckner, G.E., Howard, R.A., Koomen, M.J., Korendyke, C.M., et al.: 1995, *Solar Phys.* **162**, 357.
Burkepile, J., Darnell, T., and Tomczyk, S.: 2005, AGU abstract SH51C-1220.
Culhane, J.L., et al.: 2007, *Solar Phys.* **243**, 19.
Defise, J.M., Halain, J.P., Berghmans, D. et al.: 2007, Proc. SPIE, 6689, 66890S-12.
DeForest, C.E.: 2007, *Astrophys. J.* **661**, 532.
Delaboudinière, J.-P., Artzner, G.E., Brunaud, J., Gabriel, A.H., et al.: 1995, *Solar Phys.* **162**, 291.
Del Zanna, G., and Mason, H.E.: 2003, *Astron. Astrophys.* **406**, 1089.
Del Zanna, G.: 2008, *Astron. Astrophys.* **481**, L49.
Dere, K.P., et al.: 1997, *Astron. Astrophys. Suppl.* **125**, 149.
Feldman, U., et al.: 1992, ApJS **81**, 387.
Gelfgat, V.I., Kosarev, E.L., and Podolyak, E.R.: 1993, *Comp. Phys. Commun.* **74**, 349.
Gloeckler, G., *et al.*: 1998, *Space Sci. Rev.* **86**, 497.
Golub, L.: 2006, *Space Sci. Rev.* **124**, 23.
Golub, L., *et al.*: 2007, *Solar Phys.* **243**, 63.
Goryaev, F.F., Parenti, S., Urnov, A.M., *et al.*: 2010, *Astron. Astrophys.* **523**, 15.
Gosling, J.T., *et al.*: 1995, *Geophys. Res. Lett.* **22**, 3329.
Handy, B.N., *et al.*: 1999, *Solar Phys.* **187**, 229.
Harra, L.K., *et al.*: 2008, *Astrophys. J.* **676**, L147.
Harra, L.K., Magara, T., Hara, H., Tsuneta, S., Okamoto, T.J., and Wallace, A.J.: 2010, *Solar Phys.* **263**, 105.
Harra, L.K., Mandrini, C.H., Dasso, S., Gulisano, A.M., Steed, K., and Imada, S.: 2011, *Solar Phys.* **268**, 213.
Hefti, S., Grünwaldt, H., Bochsler, P., and Aellig, M.R.: 2000, *J. Geophys. Res.* **105**, 10527.
Howard, R.A., *et al.*: 2008, *Space Sci. Rev.* **136**, 67.
Ko, Y.K., Raymond, J.C., Zurbuchen, T.H., Riley, P., Raines, J.M., and Strachan, L.: 2006, *Astrophys. J.* **646**, 1275.
Kosugi, T., *et al.*: 2007, *Solar Phys.* **243**, 3.
Kuzin, S.V., *et al.*: 2009, *Adv. Space Res.* **43**, 1001.
Landi, E., Del Zanna, G, Young, P.R., Dere, K.P., *et al.*: 2006, *Astrophys. J. Suppl.* **162**, 261.
Landi, E. and Young, P.R.: 2009, *Astrophys. J.* **706**, 1.

Levine, R.H., Altschuler, M.D., Harvey, J.W., and Jackson, B.V.: 1977, *Astrophys. J.* **215**, 636.
Liewer, P.C., *et al.*: 2001, *J. Geophys. Res.* **106**, 15903.
Liewer, P.C., Neugebauer, M., and Zurbuchen, T.: 2003, in M. Velli, R. Bruno, F. Malara (eds.), Solar Wind Ten: Proceedings of the 10-th Int. Solar Wind Conference. AIPCP **679**, p. 51.
Liewer, P.C., Neugebauer, M., and Zurbuchen, T.: 2004, *Solar Phys.* **223**, 209.
Marsch, E., Wiegelmann, T., and Xia, L.D.: 2004, *Astron. Astrophys.* **428**, 629.
Marsch, E., Tian, H., Sun, J., Curdt, W., and Wiegelmann, T.: 2008, *Astrophys. J.* **685**, 1262.
Matsuzaki, K., Hara, H., Watanabe, T., Dere, K.P., Brown, C.M., and Culhane, L.: 2007, *Pub. Astron. Soc. Japan* **59**, S683.
Mazzotta, P., Mazzitelli, G., Colafrancesco, S., and Vittorio, N.: 1998, *Astron. Astrophys. Suppl.* **133**, 403.
McComas, D.J., *et al.*: 1998, *Space Sci. Rev.* **86**, 563.
McComas, D.J., Goldstein, R., Gosling, J.T., and Skoug, R.M.: 2001, *Space Sci. Rev.* **97**, 99.
McIntosh, S.W. and De Pontieu, B.: 2009, *Astrophys. J. Lett* **706**, L80.
Morgan, H. and Habbal, S.R.: 2007, *Astron. Astrophys.* **465**, L47.
Murray, M.J., Baker, D., van Driel-Gesztelyi, L., and Sun, J.: 2010, *Solar Phys.* **261**, 253.
Neugebauer, M., *et al.*: 1998, *J. Geophys. Res.* **103**, 14587.
Neugebauer, M., Liewer, P.C., Smith, E.J., Skoug, R.M., and Zurbuchen, T.H.: 2002, *J. Geophys. Res.* **107**, SSH 13-1.
Nitta, N.V. and De Rosa, M.L.: 2008, *Astrophys. J.* **673**, L207.
Nolte, J.T. and Roelof, E.C.: 1973, *Solar Phys.* **33**, 241.
Raymond, J.C., *et al.*: 1997, *Solar Phys.* **175**, 645.
Sakao, T., *et al.*: 2007, *Science* **318**, 1585.
Schatten, K.H., Wilcox, J.M., and Ness, N.F.: 1969, *Solar Phys.* **6**, 442.
Schrijver, C.J. and De Rosa, M.L.: 2003, *Solar Phys.* **212**, 165.
Schrijver, C.J., *et al.*: 1999, *Solar Phys.* **187**, 261.
Sheeley, N.R., *et al.*: 1997, *Astrophys. J.* **484**, 472.
Slemzin, V., *et al.*: 2008, *Ann. Geophys.* **26**, 3007.
von Steiger, R., *et al.*: 2000, *J. Geophys. Res.* **105**, 27217.
Strachan, L., Suleiman, R., Panasyuk, A.V., Biesecker, D.A., and Kohl, J.L.: 2002, *Astrophys. J.* **571**, 1008.
Švestka, Z., Fárnik, F., Hudson, H.S., and Hick, P.: 1998, *Solar Phys.* **182**, 179.
Veselovsky, I.S. and Shugay, Yu.S.: 2010, *Cosmic Research* **48**, 31.
Uchida, Y., *et al.*: 1992, *Pub. Astron. Soc. Japan* **44**, L155.
Ugarte-Urra, I., Warren, H.P., and Brooks, D.H.: 2009, *Astrophys. J.* **695**, 642.
Ugarte-Urra, I. and Warren, H.P.: 2011, *Astrophys. J.* **730:37**, 7 pp.
Urnov, A.M., Shestov, S.V., Bogachev, S.A., Goryaev, F.F., Zhitnik, I.A., and Kuzin, S.V.: 2007, *Astron. Lett.* **33**, 396.
Wang, Y.-M. and Sheeley, Jr.N.R.: 1990, *Astrophys. J.* **355**, 726.
Wang, Y.-M. and Sheeley, Jr.N.R.: 1992, *Astrophys. J.* **392**, 310.
Wang, Y.-M., Ko, Y.-K., and Grappin, R.: 2009, *Astrophys. J.* **691**, 760.
Wang, Y.-M.: 2010, *Astrophys. J.* **715**, L121.
Warren, H.P. and Brooks, D.H.: 2009, *Astrophys. J.* **700**, 762.
Warren, H.P., Ugarte-Urra, I., Young, P.R., and Stenborg, G.: 2011, *Astrophys. J.* **727:58**, 5 pp.
Winebarger, A.R., DeLuca, E.E., and Golub, L.: 2001, *Astrophys. J.* **553**, L81.
Young, P.R., Watanabe, T., Hara, H., and Mariska, J.T.: 2009, *Astron. Astrophys.* **495**, 587.